Brigham Young University
Department of Electrical and
Computer Engineering

459 Clyde Building
Provo, Utah 84602

Standard BYU QuikSCAT/SeaWinds Land/Ice Image Products

David G. Long
Brandon R. Hicks
8 Apr. 2005

MERS Technical Report # MERS 05-04
ECEN Department Report # TR-L130-05.04

Microwave Earth Remote Sensing (MERS) Laboratory

Standard BYU QuikSCAT and Seawinds Land/Ice Image Products

David G. Long
Revised By: Brandon R. Hicks
Microwave Earth Remote Sensing Laboratory
BYU Center for Remote Sensing
Brigham Young University
459 Clyde Building, Provo, UT 84602
long@ee.byu.edu (801) 422-4383

Revision 3.0
April 8, 2005

Abstract

The SeaWinds scatterometers aboard QuikSCAT and ADEOS II (Midori-2) provide normalized radar cross section (σ^o) measurements of the Earth's surface at unprecedented coverage and resolution. While originally designed for wind observation, scatterometers have proven useful in a variety of land and ice studies. To further improve the utility of the data, resolution enhancement algorithms have been developed and applied to the data. These algorithms produce images of the surface σ^o at enhanced resolution (to better than 5 km). This report briefly describes a standard product suite of QuikSCAT and SeaWinds enhanced resolution image products developed and produced at the Brigham Young University (BYU) Microwave Earth Remote Sensing (MERS) Laboratory. These data are distributed as part of the Scatterometer Climate Record Pathfinder project `http://www.scp.byu.edu`.

1 Introduction

In addition to their primary wind observation missions, scatterometers are proving essential in variety of land and ice studies [13]. Scatterometer data has proven particularly effective in cryosphere studies [13, 19] and has been applied in tropical vegetation [20] and other studies [26]. It is clear that scatterometers will continue to play an increasingly important role in monitoring tropical vegetation and polar ice in the future.

The SeaWinds scatterometer provides radar measurements of the near-surface ocean wind field with unprecedented coverage and resolution. The SeaWinds instrument makes dual polarization measurements of the normalized radar cross section (σ^o) at both vertical and horizontal polarization using a conically scanning pencil-beam antenna (see Fig. 1) [27]. The σ^o measurements have demonstrated application in a number of land and ice studies (e.g., [1, 2, 3, 6, 8, 9, 14, 15, 22, 24, 25, 26, 30]).

Two identical SeaWinds instruments have flow: one aboard the ADEOS-II (Midori-2) spaceraft and the other aboard the QuikSCAT mission. Note that by JPL convention, this instrument aboard QuikSCAT is known as QuikSCAT while SeaWinds aboard aboard ADEOS II is known as SeaWinds [29]. The Brigham Young University (BYU) Microwave Earth Remote Sensing (MERS) Laboratory has developed a standard set of land/ice image products for distribution. This report

describes these products. Both conventional and enhanced resolution products are included in the product suite. The enhanced resolution products are produced with the aid of the Scatterometer Image Reconstruction (SIR) algorithm described below.

2 The Scatterometer Image Reconstruction Algorithm

Traditionally, scatterometers have not been designed as imaging sensors. In many cases the measurements may be disjoint in the along-track dimension and usually vary somewhat in shape over the swath. By combining multiple passes and using the Scatterometer Image Reconstruction (SIR) with Filtering (SIRF) algorithm, enhanced resolution images of the surface backscatter can be produced [5, 7]. The SIR algorithm was originally developed to enhance Seasat scatterometer data[16]. The SIR algorithm has also been used with SSM/I radiometer [18] and ERS scatterometer data [13, 17]. A number of improvements to the original SIR algorithm have been developed to optimize its performance for NSCAT [7, 21].

The SIR algorithm is based on a multivariate form of block multiplicative algebraic reconstruction. Combining multiple overlapping passes and robust performance in the presence of noise, it provides enhanced resolution measurements of the surface characteristics [5]. To provide a simple intuitive explanation of the idea behind SIR, consider the following. (The incidence angle dependence of σ^o is ignored in the following discussion.) More detailed discussions are contained in [16] and [5].

Let $f(x, y)$ be a function that gives the surface σ^o at a point (x, y). The scatterometer measurement system can be modeled by

$$z = Hf + \text{noise} \tag{1}$$

where H is an operator that models the measurement system (sample spacing and aperture filtering) and z represents the measurements of σ^o made by the instrument sensor. The set of measurements z are a discrete sampling of the function f convolved with the aperture function (which may be different for each measurement). A particular measurement z_i can be written as

$$z_i = \int\int h_i(x, y)dxdy + noise \tag{2}$$

where $h_i(x, y)$ is the measurement response (due, for example, to the antenna pattern and the Doppler filter response) of the ith measurement.

For resolution enhancement, we are interested in the inverse problem:

$$\hat{f} = \hat{H}^{-1}z \tag{3}$$

where $\hat{f}$ is an estimate of f from the measurements z. The inverse of the operator H, $\hat{H}^{-1}$, is exact only if H is invertible and the measurements are noise free, in which case $\hat{f} = f$. This represents a form of resolution enhancement since information in the sidelobes of the measurement response or aperture function is recovered in the inversion. In effect, this is what the iterative SIR algorithm does, producing images at a finer resolution than the original measurements [1].

It should be noted that SIR is a true reconstruction algorithm which enables resolution enhancement algorithm by extracting information from the sidelobes of the measurement response function to generate the final image product [5]; in effect, it is an inverse reconstruction filter optimized to minimize noise in the reconstructed image.

[1]Note that the image products are produced at a particular *pixel* resolution; however, the *effective* resolution of the images is typically coarser by a factor of 2 or depending on the number of available measurements, the spatial location distribution of the measurements, temporal variations in the surface, the size of the grid, etc.

3 NSCAT

NSCAT, launched in August of 1996 is a real aperture dual polarization Ku-band radar scatterometer designed to measure the σ^o of the Earth's surface. NSCAT made dual-polarization σ^o measurements over an incidence angle range of $17° - 55°$. Over the limited incidence angle range of $\theta \in [20°, 55°]$, σ^o (in dB) is approximately a linear function of θ,

$$\sigma^o(\theta) = A + B(\theta - 40°) \tag{4}$$

where A and B are functions of surface characteristics, azimuth angle, and polarization. A is the incidence-angle normalized σ^o value at 40° incidence while B describes the dependence of σ^o on θ.

NSCAT produces nominally 25 km resolution σ^o measurements on a 25 km sampling grid. The SIRF algorithm applied to NSCAT data produces both A and B images from the NSCAT σ^o measurements. The NSCAT SIRF image pixel resolution is nominally 4.45 km with an effective resolution of 8-10 km [7, 19, 20].

While the enhanced resolution A and B images are normally of the most interest, BYU also produces a number of ancillary image products along with the enhanced resolution images. These include non-enhanced images (i.e., A and B images produced at the intrinsic resolution of the sensor), low resolution browse images, and quality assurance image products.

4 QuikSCAT and SeaWinds

Unlike NSCAT which made σ^o measurements over a broad range of incidence angles, The SeaWinds instrument makes σ^o measurements at only two nominal incidence angles, 46° and 54.1°, corresponding to the inner and outer beams. The inner beam measurement is horizontal-polarization while the outer beam is vertical-polarization. Since it is undesirable to combine measurements from different polarizations, it is not possible to infer B from the QuikSCAT and SeaWinds σ^o measurements. Instead, a single-variate form of SIR similar to the type developed for radiometer applications [18] is used to generate enhanced resolution images of σ^o (which will be termed A_v and A_h) at each of the two polarizations and nominal incidence angles of the antenna beams. Because the instrument aboard QuikSCAT and SeaWinds is nearly identical, the data, while being processed into images for each satellite individually, can also be combined. The combined data from the QuikSCAT/SeaWinds tandem mission (Tandem) is processed into Tandem images.

QuikSCAT/SeaWinds σ^o measurements are reported in two forms: termed 'eggs' and 'slices' [29, 27]. These differ in their spatial sizes and shapes. The nominal instantaneous QuikSCAT/SeaWinds antenna footprint is an ellipse. However, the on-board range-doppler processing incorporated within the instrument improves the resolution [27]. Using the on-board processor, twelve individual σ^o measurements are obtained for each footprint, though only 8 are reported in the L1B data product. These individual measurements are termed 'slices'. The slices are typically 4-6 km long (depending on the instrument mode and antenna beam) by 20 km wide. The summed measurements of the 8 center slices are known as 'egg' measurements and are reported as a standard product. The effective resolution and shape of the egg measurement nearly matches the elliptical 3 dB antenna footprint (approximately 15 km by 25 km depending on the antenna beam and instrument mode). Although lower resolution, the egg measurements have less noise are less sensitive to calibration errors. Figure 1 illustrates the SeaWinds/QuikSCAT observational geometry while Fig. 2 shows the spatial response functions of eggs and slices. Figure 3 illustrates the spatial overlap in the slices [4].

5 Standard QuikSCAT/SeaWinds/Tandem Image Products

As implemented by BYU, a number of standard QuikSCAT/SeaWinds/Tandem image products are produced. A description of these follow. The standard QuikSCAT/SeaWinds/Tandem image set consists of both SIR enhanced resolution images, as well as non-enhanced images and a number of auxiliary data images. All image products are generated and stored in the BYU MERS **SIR** file format. Viewer and reader programs for the BYU MERS **SIR** file format are available on line from the BYU NASA Scatterometer Climate Record Pathfinder web-page and anonymous ftp sites at URLs `http://www.scp.byu.edu/` and `ftp://ftp.scp.byu.edu/`, respectively. A standard file naming convention (described below) is used.

Two main divisions of QuikSCAT/SeaWinds/Tandem data products are produced from the two types of σ^o measurements reported by QuikSCAT/SeaWinds: 1) slices and 2) eggs. Separate SIR resolution enhanced and non-enhanced images are produced from each type of σ^o measurement. Egg-based SIR images have a nominal pixel resolution of 4.45 km with an estimated effective resolution of $\sim 8-10$ km. Slice-based SIR images have a nominal pixel resolution of 2.225 km with an estimated effective resolution of ~ 5 km. A set of low-resolution (5 pixels/deg) browse products are also produced.

Gridded image products are not resolution enhanced and are produced at pixel resolution of 5 times the nominal SIR resolution (11.125 km and 22.25 km for slices and eggs, respectively). Gridded images are created by accumulating all of the measurements whose center falls with a given grid element (pixel), i.e., by the "binning" or "drop in the bucket" method: for a given grid element A is generated by averaging all the measurements whose centers fall within the grid element. The resulting A values are temporal averages over the imaging time interval. Since part of the spatial response of the measurements fall outside of the grid elements (or, bins) the *effective* resolution of the gridded products is somewhat less than the grid sizes.

To aid in comparison of enhanced resolution and non-enhanced resolution products, selected gridded products are pixel replicated to produce images with the same number of pixels as the enhanced resolution products. These images are referred to as 'non' images. Figure 4 illustrates simulation results for non and SIR egg and slice images.

Standard products images are made over several standard regions identified by number, name, and a rectangular box in lat/long (see Table 1 and Figs. 5 and 6). Land images are typically produced in equal-area Lambert projection while polar images are produced in polar stereographic projection. A list of the standard image regions is given in Table 1. Polar images are based on one day's worth of data and are produced every day (see Fig. 5). Non-polar image products generally use four days of data, however one day images are also available for many regions. Non-polar images 4 day images (other than the Bering Sea region) are land masked and have ocean pixels set to the no-data value (see Fig. 6). Figures 8 and 9 compare the resolution of the various products. Figures 10 and 11 show samples of the ancillary image products. Figure 12 combines the standard regions into global values of the land/ice surface backscatter as observed by SeaWinds.

A standardized `SIR` naming scheme (described below) is used which has key information about the contents of the image file in the file name.

For a given region, the following list of SIR product files are produced for each beam. Similar products are also produced using the gridding algorithm. In addition to SIR enhanced resolution products, an 'A' product is also produced using the SIR-related AVE algorithm (see [16]) which has intermediate resolution. Each product can be produced for both slices and eggs unless otherwise indicated. The SIR algorithm is used for egg processing while the SIR algorithm with filtering (SIRF) is used for slice processing. The product type is denoted by a one character type designator in the file name.

Region Name	Region Abreviation	Lower-Left Corner Latitude	Lower-Left Corner Longitude	Upper-Right Corner Latitude	Upper-Right Corner Longitude	Region Code Number
Antarctic	Ant	-90.0	-180.0	-52.0	180.0	100
Arctic	Arc	60.0	-180.0	90.0	180.0	110
Greenland	Grn	59.0	-74.0	84.5	-11.0	202
Alaska	Ala	50.0	-180.0	73.0	-130.0	203
Cntrl-Amer	CAm	5.0	-115.0	30.0	-57.0	204
North-Amer	NAm	25.0	-135.0	65.0	-50.0	205
South-Amer	SAm	-58.0	-83.0	15.0	-32.0	206
North-Afri	NAf	2.0	-20.0	40.0	65.0	207
South-Afri	SAf	-38.0	5.0	10.0	53.0	208
Siberia	Sib	50.0	60.0	75.0	180.0	209
Europe	Eur	35.0	-12.0	72.0	65.0	210
South-Asia	SAs	5.0	60.0	30.0	130.0	211
Chin-Japan	ChJ	25.0	60.0	55.0	150.0	212
Indonesia	Ind	-15.0	93.0	10.0	165.0	213
Australia	Aus	-48.0	110.0	-10.0	180.0	214
Bering Sea	Ber	50.0	135.0	75.0	-135.0	256

Table 1: Standard product regions. The products are produced in a local radius equal-area Lambert projection, except for the Antarctic and Arctic regions (region numbers 100 and 110) which are produced in polar stereographic form.

a: A value. σ^o value in dB. For QuikSCAT/SeaWinds slices, the nominal reference incidence angles are H-pol (inner beam) 46° and V-pol (outer beam) 54.1°.

C: counts. The number of σ^o measurements which hit the pixel during the imaging interval. (produced for only slices)

E: mean reconstruction error in dB. The mean difference between each measurement which hits the pixel and its forward projection based on the final image estimate.

I: incidence angle standard deviation in deg. The standard deviation is over all the σ^o measurements which hit the pixel during the imaging interval.

J: mean incidence angle in deg. The mean is over all the σ^o measurements which hit the pixel during the imaging interval.

p: time image (in minutes from the start of the imaging interval). The time value reports the effective time center of the measurements used to compute the image [28, 10].

V: reconstruction std image (in dB). The standard deviation of the difference between each measurement which hits the pixel and its forward projection based on the final image estimate. Useful for evaluating temporal variation in the surface, azimuth modulation, etc.

A sample product listing of the standard products is contained in the Appendix. Table 2 gives the approximate file sizes for the egg-derived product files for each region. Slice-derived products are approximately 4 times larger.

Table 2: Approximate QuikSCAT/SeaWinds/Tandem standard product file sizes for egg-derived products in MB for each region. Slice-derived products are approximately 4 times larger due to the higher resolution of the products.

Region Abreviation	Region Code Number	SIR/SIRF Image size (MB)	Gridded Image size (MB)	Region Name
Ant	100	7.5	3.0	Antarctic
Arc	110	4.7	1.9	Arctic
Grn	202	1.1	0.5	Greenland
Ala	203	1.0	0.4	Alaska
CAm	204	2.0	0.8	Cntrl-Amer
NAm	205	4.3	1.8	North-Amer
SAm	206	4.8	2.0	South-Amer
NAf	207	4.8	2.0	North-Afri
SAf	208	3.1	1.2	South-Afri
Sib	209	2.8	1.1	Siberia
Eur	210	3.2	1.3	Europe
SAs	211	2.5	1.0	South-Asia
ChJ	212	3.8	1.5	Chin-Japan
Ind	213	2.4	1.0	Indonesia
Aus	214	3.8	1.5	Australia
Ber	256	0.1	0.1	Bering Sea

6 User Notes

This section provides additional specific details regarding the generation and application of the standard QuikSCAT/SeaWinds/Tandem products. SIR images are generated from QuikSCAT/SeaWinds L1B files.

In generating enhanced resolution images, the SIR algorithm combines σ^o measurements (only measurements from a single beam are combined) from multiple azimuth angles and (possibly) multiple orbit passes collected over the imaging period. The resulting images represent a non-linear weighted average of the measurements [5]. There is an implicit assumption that the surface characteristics remain constant over the imaging period. We note that since that ocean changes rapidly, imaging artifacts are often observed in SIR images over the ocean. Azimuth dependence in the scattering and/or changes during the imaging period (e.g. due to melt) can also lead to imaging artifacts.

The effective resolution of the enhanced resolution images depends on the number of measurements and the precise details of their overlap, orientation, spatial locations. The effective measurement observation time is provided in the **p** image [28, 10].

6.1 Quality flags and σ^o measurements used

Only σ^o measurements flagged as 'usable' in the QuikSCAT/SeaWinds L1B files are included in the processing. Note that the SIR algorithm forms images in dB space and thus excludes use of negative σ^o measurements. Since most land/ice areas have fairly large σ^o, relatively few measurements are excluded.

While 8 slice measurements per pulse are reported in the L1B file, the outer slices tend to more noisy than the inner slices and are more sensitive to calibration/balance problems. For this reason

only the center 6 slices are typically used in slice image products.

6.2 Ascending/Descending pass images

Ordinarily, both ascending and descending data passes are combined in creating the images. This, in effect, assumes that the surface is essentially the same for both ascending and descending passes, equivalent to assuming that the diurnal variation is small since ascending and descending passes are approximately 12 hours apart at the equator. (Time samples are closer at the poles [10].) However, some diurnal variations have been observed, particularly in the polar regions during peak melting periods. To aid the study of diurnal variations, additional products are produced which use only ascending and descending data. The naming scheme reflects this.

6.3 Local time-of-day (Morning/Mid-day/Evening) images

It has been found that the separating the data into ascending and descending pass-only data in high latitude regions has some undesirable effects on the temporal resolution of the resulting images [10]. In order to achieve better time sampling in these regions, a new method has been developed. This new method separates the data into morning and evening data, on the basis of the measurement local time of day. For QuikSCAT, data is separated at 12 AM and 12 PM, local time, into two images representing the morning, and evening of each day. Morning and evening images created using this method provide more precise temporal sampling, and therefore aid the study of diurnal variations in the polar regions. These are produced for the polar regions, and may be produced for other selected regions. Due to the difference in time-of-ascending node for SeaWinds, the data is divided at 8 AM and 4 PM.

Using tandem QuikSCAT and SeaWinds data, additional images are produced for selected regions: ith Tandem images the image set also includes midday images, thus providing three images per day in these regions [11]. These images use a similar naming scheme as the QuikSCAT only morning/evening images, however the definitions differ slightly. Tandem morning images only cover data from 12 AM to 8 AM local time, and evening images only cover data from 4 PM to 12 AM local time. Tandem midday images cover the interim, from 8 AM to 4 PM local time. These images provide nearly uniform samples three times a day, allowing higher frequency diurnal variations to be resolved.

The indicators used in the file naming scheme are given in Table 5. It should be noted that under the naming scheme described in section 7.1, there are some nuances that need explanation for these images. Since this method divides the data based on the local time of measurements, the data used to create these images come from time periods greater than 24 hours. This makes the naming of these images somewhat complicated. Though each pixel in the image is guaranteed to be created from a narrow time period, the range of times depends on the pixel. As a result, the images use data from 32-36 hours of data and therefore, are labeled as two-day images. Consequently, DY2 is always the day after DY1 for these images. Because **p** images (code 11) do not support negative time values, the evening image is the first chronologically, followed by the morning, and the midday (where applicable). Consequently, the evening image can be viewed as evening of DY1, and the morning/midday as that of DY2.

6.4 Antenna azimuth angles

Note that due to the rotation of the antenna, the cross-track density of σ^o measurements varies with more measurements at the outer edges of the swath than at the swath center. As a result, swath edges are clearly visible in the count images.

Note that in producing the images the forward-looking and aft-looking measurements are combined and the resulting average is over the various azimuth angles of the measurements. The azimuth angles of the measurements hitting a given location vary with the pixel location and with time and may be further affected by missing or low-quality data. While most land and sea-ice regions exhibit little variation in σ^o with azimuth angle, σ^o in some regions (notably, parts of East Antarctica) is dependent on the azimuth angle of the observations. Since σ^o measurements from multiple azimuth angles may be combined, the resulting image value is sensitive to the azimuth angle distribution of the measurements. This effect can result in artifacts near the edge of the swath. In this area the σ^o measurements span a large range of azimuth angles. Thus, to improve the image quality, σ^o measurements in the outer edges of each beam's swath are not used to generate the SIR image products. σ^o measurements with antenna azimuth angles within $\pm 15^\circ$ of orthogoal to the flight path are discarded prior to applying SIR. The $\pm 15^\circ$ threshold was subjectively chosen based on a tradeoff of computation and image artifact reduction. While eliminating far swath σ^o measurements reduces the swath width somewhat, the swath width reduction is small and results in a substantial reduction in computational time required to generate the enhanced resolution images.

6.5 Coverage

QuikSCAT and SeaWinds are both in a near-four day repeat orbit. While 90% of the Earth's oceans are covered in one day, the frequency of swath coverage is highly latitude dependent with most frequent passes near the poles. (Note that while the V pol beam covers the exact poles, the H pol beam does not.) It takes a minimum of two days to provide complete coverage of the Earth's surface. For this reason, several days of data (typically 4, to obtain the maximum diversity) are used for non-polar regions. In some non-polar regions, single day images are also made to enable better temporal resolution.

While relatively rare, missing L1B data can result in "holes" in the image products and/or reduced resolution enhancement. This can lead to errors in sea ice extent maps.

6.6 Slice balancing and topographic effects

No special calibration correction is applied to the L1B σ^o measurements. The X factor used in computing the σ^o measurement from the raw power measurements is somewhat dependent on the height of the surface. JPL's processing includes a correction factor to account for this. The correction is estimated to be accurate to within 0.15 dB. A correction is also applied for the measurement location. While the spatial response function is somewhat dependent on the surface height, this dependence is ignored in image formation.

6.7 Incidence angle correction

The observed variation in incidence angle of the σ^o measurements over a given region is very small, typically less than 0.1°. For comparison, over vegetated regions typically B[the variation in σ^o with incidence angle, see Eq. (1)] is ~ -0.13 dB/deg. For ice this may be as large as 0.25 dB/deg. (Over the ocean $B\sim$ 1 dB/deg.) Since only σ^o measurements from a given beam are combined and the egg incidence angle variation is small, incidence angle normalization is felt to be unnecessary at this time for egg images and no σ^o incidence angle correction is made; thus, the image A values correspond to the σ^o value at the beam incidence angle. For slice images, individual slice σ^o measurements are incidence angle corrected to the nominal reference angle using a B value of ~ -0.13 dB/deg. The mean incidence angle (**I**) and the standard deviation (**J**) of incidence angles of the measurements for each pixel are reported.

6.8 Auxiliary Images

In addition to the standard images produced, there are a number of auxiliary images made for each region to aid the use of the standard images. In addition to images representing latitude and longitude, land mask, pixel area (polar regions only), and topography images are available for each standard region.

Most of the standard regions use conformal (equal-area) projections. For such projections, the area of each pixel is constant and equation to the nominal pixel dimension (4.45 km for eggs, 2.225 km for slices) squared. However, polar regions use a polar stereographic projection. This projection does not have constant area pixels. For these regions, SIR-format images that contain the pixel area in square km for each pixel are provided. These images are called area images or **Z** images.

7 BYU `SIR` File Format

The BYU-MERS `SIR` image format was developed by the Brigham Young University (BYU) Microwave Earth Remote Sensing (MERS) laboratory to store a variety of types and projections of EArth images along with the information required to earth-locate the image pixels.

A `SIR` format file consists of one or more 512 byte headers followed by the image data and additional zero padding to insure the file is a multiple of 512 bytes long[2]. The file header record contains all of the information required to read the remainder of the file and the map projection information required to map pixels to lat/long coordinates on the Earth surface. The image pixel values generally represent floating point values and may be stored in one of three ways. The primary method is as 2 byte integers (with the high order byte first), though the pixels may be stored as single bytes or IEEE floating point values. Scale factors are stored in the header to convert the integer or byte pixel values to native floating point units. The image is stored in row-scanned (left to right) order from the lower left corner (which is the origin of the image) up through the upper right corner. By default, the location of a pixel is identified with its lower-left corner. The origin of pixel (1,1) is the lower left corner of the image. The array index n of the $(i,j)^{th}$ pixel where i is horizontal and j is vertical is given by $n = (j-1) * N_x + i$ where N_x is the horizontal dimension of the image. The last pixel stored in the file is at (N_x, N_y).

The `SIR` file header contains various numerical values and strings which describe the image contents. For example, a no-data flag value is set within the header as well as the nominal display range and the minimum and maximum representable values. Optional secondary header records (512 bytes) can be used to store additional, non-standard information.

The standard `SIR` file format supports a variety of image projections including:

1. Rectangular array (no projection)
2. A rectangular lat/lon array
3. Two different types of Lambert equal-area projections which can be used in either non-polar or polar projections
4. Polar stereographic projections
5. EASE grid polar projection with various resolutions
6. EASE global projection with various resolutions

[2]This ensures that images can be transferred to and from all platforms without loss using binary ftp.

Table 3: Standard sensor strings for `SIR` file names. Special symbols XX, Y, D, E, G, and P are defined in Tab. 5.

$SENS$	Sensor
ers1	ERS-1 AMI scatterometer mode
ers2	ERS-2 AMI scatterometer mode
FXXY	SSM/I FXX, channel index Y
nsDP	NSCAT
qDEP	SeaWinds on QuikSCAT (QuikSCAT)
sDEP	SeaWinds on ADEOS II (SeaWinds)
tDEP	tandem QuikSCAT and SeaWinds (Tandem)
sas$P$	SASS
trmm	TRMM PR surface σ^o
topo	topography map

For the QuikSCAT/SeaWinds/Tandem products described here, only the Lambert and polar stereographic projections are used.

Readers for the `SIR` file format are available in C, C++, FORTRAN, Matlab, and IDL/PVWAVE. Viewer and reader programs are available on line from the BYU MERS web and anonymous ftp sites at URLs `http://scp.byu.edu/downloads.html` and `ftp://ftp.scp.byu.edu/software/`, respectively[3]. Documentation for these readers are located there. Sample files and various utility and display routines are also available. (Be sure to use binary ftp to transfer `.sir` files!)

A customized version of **xv** which reads `.sir` files and can convert images to other forms is also available on this site. Routines for display in Matlab and IDL/PV-Wave are available at the site. Adobe Photoshop can display the image data `.sir` file stored as two-byte integers. Read the file as 'raw', specify a 512 header and 16 bit data, and enter the image dimensions in pixels.

7.1 `SIR` Standard file name format

Where possible, a standardized file naming scheme for `SIR` format files, suitable for linux/unix, irix, vms, and windows 9X and above. The general naming scheme is:

$$SENS - T - \mathbf{REG}YR - DY1 - DY2.RCN$$

where $SENS$ is the four character sensor name in Table 3, T is the one character image type code given in Table 4, **REG** is a region identifier string, YR is a two digit year code, $DY1$ and $DY2$ are the three digit Julian day-of-the-year of the data used to make the image, and RCN is the reconstruction type file extension given in Table 6. A number of three character region identification strings are listed in Table 8. Special product files may use other longer strings for the region name. Optionally, additional file extensions may be appended to the standard name to denote a post-processed image (see Table 7). Standard grid sizes are listed in Table 9.

[3]The reader code may be copied and modified and freely distributed so long as (1) original or modified code is not redistributed for profit and (2) acknowledgment is made that the original code was obtained from the Microwave Earth Remote Sensing Laboratory at Brigham Young University, Provo, UT.

Table 4: Selected standard type codes for `SIR` file names

T (type)	Code Number	Description
a	1	A image (σ^o in dB at reference incidence angle)
b	2	B image (slope of sigma-0 in dB/deg) (N/A for QuikSCAT/Seawinds)
C	8	counts or hits (measurements) per pixel
E	21	average reconstruction error image (dB)
h	19	height (in m)
I	7	incidence angle standard deviation (in deg)
J	9	average incidence angle (in deg)
m	0	mask image
p	11	pixel time estimate (min from start of image interval)
V	22	reconstruction error standard deviation image (dB)
x	3	longitude image (deg)
y	31	latitude image (deg)
z	45	angle of grid w/respect to north (deg)
Z	44	pixel area (km^2)

Table 5: Standard sensor string characters used in standard file naming scheme in Tab. 3.

Symbol	Valid Values	Definition
XX	10-14	DMSP platform identifier
Y	1-7	SSM/I channel number
		(1=19H, 2=19V, 3=22, 4=37H, 5=37V, 6=85H, 7=85V)
D	c,u,a,d,	Ascending/descending pass indicator
	m,n,e	Local time-of-day indicator
		c: All data used (NSCAT)
		u: All data used (QuikSCAT & Tandem)
		q: All data used (Tandem)
		w: All used (SeaWinds)
		a: Ascending orbit pass data only used
		d: Descending orbit pass data only used
		m: Morning data only used
		n: Midday data only used
		e: Evening data only used
E	e,s	Egg/Slice indicator (QuikSCAT/SeaWinds/Tandem only)
		e: QuikSCAT/SeaWinds/Tandem egg σ^o measurements
		s: QuikSCAT/SeaWinds/Tandem slice σ^o measurements
P	h,v	Polarization flag

Table 6: Standard reconstruction algorithm extensions for `SIR` file names

RCN	Standard reconstruction technique
.sir	SIR or SIRF algorithm
.ave	AVE image algorithm
.non	non-enhanced
.grd	gridded
.brw	low resolution gridded browse image

Table 7: Standardized extra file extensions for `SIR` file names. These are optional.

Extension	Description
.lmsk	land masked data image (ocean set to no-data value)
.lmask	land mask (0=Ocean, 1=land)
.mask	general mask image
.imsk	Ice masked image
.omsk	Ocean masked image
.dif	Difference image
.gz	gzipped file
.sr	Subregion extracted image
.ed	Manually edited image
.lmask	binary land mask image

Table 8: Standard three character region abbreviation strings for `SIR` file names

REG	Code Number	Description
Ama	1	Amazon
Ant	100	Antarctica
Arc	110	Artic
Grn	202	Greenland
Ala	203	Alaska
CAm	204	Central America
NAm	205	North America
SAm	206	South America
NAf	207	North Africa
SAf	208	South Africa
Sib	209	Siberia
Eur	210	Europe
SAs	211	South Asia
ChJ	212	China-Japan
Ind	213	Indonesia
Aus	214	Australia
Ber	256	Bering Sea

Table 9: Standard `SIR` image grid sizes

Sensor	SIR*/AVE	GRD
ERS-1/2	8.9 km	44.5 km
SASS	4.45 km	22.25 km
NSCAT	4.45 km	22.25 km
QuikSCAT/SeaWinds/Tandem (egg)	4.45 km	22.25 km
QuikSCAT/SeaWinds/Tandem (slice)	2.225 km	11.125 km

* Note: SASS, NSCAT, and QuikSCAT/SeaWinds/Tandem (slice) use the SIRF algorithm (SIR w/median filtering) while ERS-1/2 and QuikSCAT/SeaWinds/Tandem (egg) use the SIR algorithm (w/o median filtering) [5].

References

[1] H.S. Anderson and D.G. Long, "Sea Ice Mapping Method for SeaWinds," *IEEE Transactions on Geoscience and Remote Sensing*, Vol. 43, No. 3, pp. 647-657, 2005.

[2] I.S. Ashcraft and D.G. Long, "SeaWinds Views Greenland," *Proc. Int. Geosci. Rem. Sens. Sym.*, Honolulu, Hawaii, 6-10 July, 2000.

[3] I.S. Ashcraft and D.G. Long, "Observation and Characterization of Radar Backscatter over Greenland," *IEEE Transactions on Geoscience and Remote Sensing*, Vol. 43, No. 2, pp 237-246, 2005.

[4] I.S. Ashcraft and D.G. Long, "The spatial response function of SeaWinds backscatter measurements", in "Earth Observations Systems VIII", W.L. Barnes, ed., *Proceedings of SPIE Vol. 5151*, pp. 609-618, 3-6 Aug 2003. See also, `http://www.scp.byu.edu/software/Xshape/Xshape.html`

[5] D.S. Early and D.G. Long, "Image Reconstruction and Enhanced Resolution Imaging from Irregular Samples," *IEEE Trans. Geosci. Remote Sens.*, Vol. 39, No. 2, pp. 291-302, 2001.

[6] M.R. Drinkwater, D.G. Long, and A.W. Bingham, "Greenland Snow Accumulation Estimates from Scatterometer Data," *Journal of Geophysical Research*, Vol. 106, No. D24, pp. 33935-33950, 2001.

[7] J. Dyal and D.G. Long, "NSCAT Views the Earth," MERS Technical Report, # MERS 97-004, Brigham Young University, 21 Oct. 1997. Available on the web at `http://www.mers.byu.edu/Papers/mers_reports.html`

[8] R.R. Forster, D.G. Long, K.C. Jezek, S.D. Drobot, and M.R. Anderson, "The Onset of Arctic Sea-Ice Snowmelt as Detected with Passive- and Active-microwave Remote Sensing," *Annals of Glaciology*, Vol. 33, pp. 85-93, 2001.

[9] J. Haarpainter, R.T. Tonboe, D.G. Long and M. L. VanWoert, "Automatic Detection and Validity of the Sea Ice Edge: An Application of Enhanced Resolution QuikScat/SeaWinds Data," *IEEE Transactions on Geoscience and Remote Sensing*, Vol. 42, No. 7, pp. 1433-1443, 2004.

[10] B.R. Hicks and D.G. Long, "Improving Temporal Resolution of SIR Images for QuikSCAT in the Polar Regions", MERS Technical Report 05-02, Brigham Young University, March, 2005. Available on the web at `http://www.mers.byu.edu/Papers/mers_reports.html`

[11] B.R. Hicks and D.G. Long, "Improving Temporal Resolution of SIR Images for Tandem Mission in the Polar Regions", MERS Technical Report 05-03, Brigham Young University, March, 2005. Available on the web at `http://www.mers.byu.edu/Papers/mers_reports.html`

[12] D.G. Long, J. Ballantyne, and C. Bertoia, "Is the Number of Icebergs Really Increasing?" *EOS, Transactions of the American Geophysical Union*, Vol. 83, No. 42, pp. 469 & 474, 15 Oct. 2002.

[13] D.G. Long, M.R. Drinkwater, B. Holt, S. Saatchi, and C. Bertoia, "Global Ice and Land Climate Studies Using Scatterometer Image Data," *EOS, Transaction of the American Geophysical Union*, Vol. 82, No. 43, pg. 503, 23 Oct. 2001.

[14] D.G. Long and M.R. Drinkwater, "Azimuth Variation in Microwave Scatterometer and Radiometer Data Over Antarctica," *IEEE Trans. Geosci. Remote Sens.*, Vol. 38, No. 4, pp. 1857-1870, 2000.

[15] D.G. Long, "Land and Ice Applications of SeaWinds Data," *Proc. Int. Geosci. Rem. Sens. Sym.*, Honolulu, Hawaii, 6-10 July, pp. 1220–1222, 2000.

[16] D.G. Long, P. Hardin, and P. Whiting, "Resolution Enhancement of Spaceborne Scatterometer Data," *IEEE Trans. Geosci. Remote Sens.*, vol. 31, pp. 700–715, 1993.

[17] D.G. Long, D. Early, and M.R. Drinkwater, "Enhanced Resolution ERS-1 Scatterometer Imaging of Southern Hemisphere Polar Ice," *Proc. Int. Geosci. Rem. Sens. Sym.*, Pasadena, California, 8-12 August, pp. 156–158, 1994.

[18] D.G. Long and D. Daum,"Spatial Resolution Enhancement of SSM/I Data," *IEEE Trans. Geosci. Rem. Sens.*, vol. 36, pp. 407–417, 1997.

[19] D.G. Long and M.R. Drinkwater, "Cryosphere Applications of NSCAT Data," *IEEE Trans. Geosci. Remote Sens.*, Vol. 37, No. 3, pp. 1671-1684, 1999.

[20] D.G. Long, "NSCAT Views Land and Ice," *Proc. Int. Geosci. Rem. Sens. Sym.*, pp. 1973-1975, Seattle, Washington, 6-10 July, 1998.

[21] Q.P. Remund and D.G. Long, "Optimization of SIRF for NSCAT," MERS Technical Report # MERS 97-003, Brigham Young University, 3 July 1997. Available on the web at `http://www.mers.byu.edu/Papers/mers_reports.html`

[22] Q.P. Remund and D.G. Long, "Polar Sea Ice Extent Mapping Using Ku-Band Scatterometer Data," *J. Geophys. Res.*, Vol. 104, No. C5, pp. 11515-11527, 1999.

[23] Q.P. Remund and D.G. Long, "Sea Ice Mapping Algorithm for QuikSCAT and Seawinds," *Proc. Int. Geosci. Rem. Sens. Sym.*, pp. 1686-1688, Seattle, Washington, 6-10 July, 1998.

[24] Q.P. Remund and D.G. Long, "Large-scale Inverse Ku-band Backscatter Modeling of Sea Ice," *IEEE Transactions on Geoscience and Remote Sensing*, Vol. 41, No. 8, pp. 1821-1832, 2003.

[25] Q.P. Remund and D.G. Long, "Iterative Estimation of Antarctic Sea Ice Extent Using SeaWinds Data," *Proc. Int. Geosci. Rem. Sens. Sym.*, Honolulu, Hawaii, pp. 491-493, 6-10 July, 2000.

[26] H. Stephen and D.G. Long, "Microwave Backscatter Modeling of Erg Surfaces in the Sahara Desert," *IEEE Transactions on Geoscience and Remote Sensing*, Vol. 43, No. 2, pp. 238-247, 2005.

[27] M.W. Spencer, C. Wu, and D.G. Long, "Improved Resolution Backscatter Measurements with the SeaWinds Pencil-Beam Scatterometer," *IEEE Transactions on Geoscience and Remote Sensing,* Vol. 38, No. 1, pp.89-104, 2000.

[28] G. Watt and D.G. Long, "Temporal Average Estimate Algorithm for ERS-1/2," MERS Technical Report, # MERS 97-07, Brigham Young University, 5 Aug. 1997. Available on the web at `http://www.mers.byu.edu/Papers/mers_reports.html`

[29] "SeaWinds/QuikSCAT Users Guide", SeaWinds Project Office, Jet Propulsion Laboratory, Padadena, CA, 1999.

[30] Y. Zhao, A.K. Liu, and D.G. Long, "Validation of Sea Ice Motion from QuikSCAT with Those from SSM/I and Buoy," *IEEE Transactions on Geoscience and Remote Sensing*, Vol. 40, No. 6, pp. 1241-1246, 2002.

A Sample QuikSCAT Product Listing

The following is a sample listing of the egg product files for the h pol beam. Similar products are produced for the v pol beam and for SeaWinds and Tandem mission. Note that files with a `.non` extension contain the same data as the corresponding `.grd` file but the gridded data pixels have been replicated to produce images the same size as the `.sir` images. Browse (low resolution grided data) products have a `.brw` extension and are not land or ice masked. Selected products are also produced from slices, in which case the sensor prefix is 'qus' rather than 'que'.

Browse Products

```
queh-a-Glb99-001-001.brw
queh-V-Glb99-001-001.brw
queh-C-Glb99-001-001.brw
quev-a-Glb99-001-001.brw
quev-V-Glb99-001-001.brw
quev-C-Glb99-001-001.brw
```

Enhanced resolution and Grid Products

```
queh-C-Ala99-001-001.grd.lmsk
queh-C-Ant99-001-001.grd
queh-C-Arc99-001-001.grd
queh-C-Aus99-001-001.grd.lmsk
queh-C-Ber99-001-001.grd
queh-C-CAm99-001-001.grd.lmsk
queh-C-ChJ99-001-001.grd.lmsk
queh-C-Eur99-001-001.grd.lmsk
queh-C-Grn99-001-001.grd.lmsk
queh-C-Ind99-001-001.grd.lmsk
queh-C-NAf99-001-001.grd.lmsk
queh-C-NAm99-001-001.grd.lmsk
queh-C-SAf99-001-001.grd.lmsk
queh-C-SAm99-001-001.grd.lmsk
queh-C-SAs99-001-001.grd.lmsk
queh-C-Sib99-001-001.grd.lmsk
queh-E-Ala99-001-001.sir.lmsk
queh-E-Ant99-001-001.sir
queh-E-Arc99-001-001.sir
queh-E-Aus99-001-001.sir.lmsk
queh-E-Ber99-001-001.sir
queh-E-CAm99-001-001.sir.lmsk
queh-E-ChJ99-001-001.sir.lmsk
queh-E-Eur99-001-001.sir
queh-E-Eur99-001-001.sir.lmsk
queh-E-Grn99-001-001.sir.lmsk
queh-E-Ind99-001-001.sir.lmsk
queh-E-NAf99-001-001.sir.lmsk
queh-E-NAm99-001-001.sir.lmsk
queh-E-SAf99-001-001.sir.lmsk
queh-E-SAm99-001-001.sir.lmsk
queh-E-SAs99-001-001.sir.lmsk
queh-E-Sib99-001-001.sir.lmsk
queh-I-Ala99-001-001.grd.lmsk
queh-I-Ala99-001-001.sir.lmsk
queh-I-Ant99-001-001.grd
queh-I-Ant99-001-001.sir
queh-I-Arc99-001-001.grd
queh-I-Arc99-001-001.sir
queh-I-Aus99-001-001.grd.lmsk
queh-I-Aus99-001-001.sir.lmsk
queh-I-Ber99-001-001.grd
queh-I-Ber99-001-001.sir
queh-I-CAm99-001-001.grd.lmsk
queh-I-CAm99-001-001.sir.lmsk
queh-I-ChJ99-001-001.grd.lmsk
queh-I-ChJ99-001-001.sir.lmsk
queh-I-Eur99-001-001.grd.lmsk
queh-I-Eur99-001-001.sir.lmsk
queh-I-Grn99-001-001.grd.lmsk
queh-I-Grn99-001-001.sir.lmsk
queh-I-Ind99-001-001.grd.lmsk
queh-I-Ind99-001-001.sir.lmsk
queh-I-NAf99-001-001.grd.lmsk
queh-I-NAf99-001-001.sir.lmsk
queh-I-NAm99-001-001.grd.lmsk
queh-I-NAm99-001-001.sir.lmsk
queh-I-SAf99-001-001.grd.lmsk
queh-I-SAf99-001-001.sir.lmsk
queh-I-SAm99-001-001.grd.lmsk
queh-I-SAm99-001-001.sir.lmsk
queh-I-SAs99-001-001.grd.lmsk
queh-I-SAs99-001-001.sir.lmsk
queh-I-Sib99-001-001.grd.lmsk
queh-I-Sib99-001-001.sir.lmsk
queh-J-Ala99-001-001.grd.lmsk
queh-J-Ala99-001-001.sir.lmsk
```

```
queh-J-Ant99-001-001.grd
queh-J-Ant99-001-001.sir
queh-J-Arc99-001-001.grd
queh-J-Arc99-001-001.sir
queh-J-Aus99-001-001.grd.lmsk
queh-J-Aus99-001-001.sir.lmsk
queh-J-Ber99-001-001.grd
queh-J-Ber99-001-001.sir
queh-J-CAm99-001-001.grd.lmsk
queh-J-CAm99-001-001.sir.lmsk
queh-J-ChJ99-001-001.grd.lmsk
queh-J-ChJ99-001-001.sir.lmsk
queh-J-Eur99-001-001.grd.lmsk
queh-J-Eur99-001-001.sir.lmsk
queh-J-Grn99-001-001.grd.lmsk
queh-J-Grn99-001-001.sir.lmsk
queh-J-Ind99-001-001.grd.lmsk
queh-J-Ind99-001-001.sir.lmsk
queh-J-NAf99-001-001.grd.lmsk
queh-J-NAf99-001-001.sir.lmsk
queh-J-NAm99-001-001.grd.lmsk
queh-J-NAm99-001-001.sir.lmsk
queh-J-SAf99-001-001.grd.lmsk
queh-J-SAf99-001-001.sir.lmsk
queh-J-SAm99-001-001.grd.lmsk
queh-J-SAm99-001-001.sir.lmsk
queh-J-SAs99-001-001.grd.lmsk
queh-J-SAs99-001-001.sir.lmsk
queh-J-Sib99-001-001.grd.lmsk
queh-J-Sib99-001-001.sir.lmsk
queh-V-Ala99-001-001.grd.lmsk
queh-V-Ala99-001-001.non.lmsk
queh-V-Ala99-001-001.sir.lmsk
queh-V-Ant99-001-001.grd
queh-V-Ant99-001-001.non
queh-V-Ant99-001-001.sir
queh-V-Arc99-001-001.grd
queh-V-Arc99-001-001.non
queh-V-Arc99-001-001.sir
queh-V-Aus99-001-001.grd.lmsk
queh-V-Aus99-001-001.non.lmsk
queh-V-Aus99-001-001.sir.lmsk
queh-V-Ber99-001-001.grd
queh-V-Ber99-001-001.non
queh-V-Ber99-001-001.sir
queh-V-CAm99-001-001.grd.lmsk
queh-V-CAm99-001-001.non.lmsk
queh-V-CAm99-001-001.sir.lmsk
queh-V-ChJ99-001-001.grd.lmsk
queh-V-ChJ99-001-001.non.lmsk
queh-V-ChJ99-001-001.sir.lmsk
queh-V-Eur99-001-001.grd.lmsk
queh-V-Eur99-001-001.non.lmsk
queh-V-Eur99-001-001.sir.lmsk
queh-V-Grn99-001-001.grd.lmsk
queh-V-Grn99-001-001.non.lmsk
queh-V-Grn99-001-001.sir.lmsk
queh-V-Ind99-001-001.grd.lmsk
queh-V-Ind99-001-001.non.lmsk
queh-V-Ind99-001-001.sir.lmsk
queh-V-NAf99-001-001.grd.lmsk
queh-V-NAf99-001-001.non.lmsk
queh-V-NAf99-001-001.sir.lmsk
queh-V-NAm99-001-001.grd.lmsk
queh-V-NAm99-001-001.non.lmsk
queh-V-NAm99-001-001.sir.lmsk
queh-V-SAf99-001-001.grd.lmsk
queh-V-SAf99-001-001.non.lmsk
queh-V-SAf99-001-001.sir.lmsk
queh-V-SAm99-001-001.grd.lmsk
queh-V-SAm99-001-001.non.lmsk
queh-V-SAm99-001-001.sir.lmsk
queh-V-SAs99-001-001.grd.lmsk
queh-V-SAs99-001-001.non.lmsk
queh-V-SAs99-001-001.sir.lmsk
queh-V-Sib99-001-001.grd.lmsk
queh-V-Sib99-001-001.non.lmsk
queh-V-Sib99-001-001.sir.lmsk
queh-a-Ala99-001-001.ave.lmsk
queh-a-Ala99-001-001.grd.lmsk
queh-a-Ala99-001-001.non.lmsk
queh-a-Ala99-001-001.sir.lmsk
queh-a-Ant99-001-001.ave
queh-a-Ant99-001-001.grd
queh-a-Ant99-001-001.non
queh-a-Ant99-001-001.sir
queh-a-Arc99-001-001.ave
queh-a-Arc99-001-001.grd
queh-a-Arc99-001-001.non
queh-a-Arc99-001-001.sir
queh-a-Aus99-001-001.ave.lmsk
queh-a-Aus99-001-001.grd.lmsk
queh-a-Aus99-001-001.non.lmsk
queh-a-Aus99-001-001.sir.lmsk
queh-a-Ber99-001-001.ave
queh-a-Ber99-001-001.grd
```

queh-a-Ber99-001-001.non
queh-a-Ber99-001-001.sir
queh-a-CAm99-001-001.ave.lmsk
queh-a-CAm99-001-001.grd.lmsk
queh-a-CAm99-001-001.non.lmsk
queh-a-CAm99-001-001.sir.lmsk
queh-a-ChJ99-001-001.ave.lmsk
queh-a-ChJ99-001-001.grd.lmsk
queh-a-ChJ99-001-001.non.lmsk
queh-a-ChJ99-001-001.sir.lmsk
queh-a-Eur99-001-001.ave.lmsk
queh-a-Eur99-001-001.grd.lmsk
queh-a-Eur99-001-001.non.lmsk
queh-a-Eur99-001-001.sir.lmsk
queh-a-Grn99-001-001.ave.lmsk
queh-a-Grn99-001-001.grd.lmsk
queh-a-Grn99-001-001.non.lmsk
queh-a-Grn99-001-001.sir.lmsk
queh-a-Ind99-001-001.ave.lmsk
queh-a-Ind99-001-001.grd.lmsk
queh-a-Ind99-001-001.non.lmsk
queh-a-Ind99-001-001.sir.lmsk
queh-a-NAf99-001-001.ave.lmsk
queh-a-NAf99-001-001.grd.lmsk
queh-a-NAf99-001-001.non.lmsk
queh-a-NAf99-001-001.sir.lmsk
queh-a-NAm99-001-001.ave.lmsk
queh-a-NAm99-001-001.grd.lmsk
queh-a-NAm99-001-001.non.lmsk
queh-a-NAm99-001-001.sir.lmsk
queh-a-SAf99-001-001.ave.lmsk
queh-a-SAf99-001-001.grd.lmsk
queh-a-SAf99-001-001.non.lmsk
queh-a-SAf99-001-001.sir.lmsk
queh-a-SAm99-001-001.ave.lmsk
queh-a-SAm99-001-001.grd.lmsk
queh-a-SAm99-001-001.non.lmsk
queh-a-SAm99-001-001.sir.lmsk
queh-a-SAs99-001-001.ave.lmsk
queh-a-SAs99-001-001.grd.lmsk
queh-a-SAs99-001-001.non.lmsk
queh-a-SAs99-001-001.sir.lmsk
queh-a-Sib99-001-001.ave.lmsk
queh-a-Sib99-001-001.grd.lmsk
queh-a-Sib99-001-001.non.lmsk
queh-a-Sib99-001-001.sir.lmsk
queh-p-Ala99-001-001.grd.lmsk
queh-p-Ala99-001-001.sir.lmsk
queh-p-Ant99-001-001.grd
queh-p-Ant99-001-001.sir
queh-p-Arc99-001-001.grd
queh-p-Arc99-001-001.sir
queh-p-Aus99-001-001.grd.lmsk
queh-p-Aus99-001-001.sir.lmsk
queh-p-Ber99-001-001.grd
queh-p-Ber99-001-001.sir
queh-p-CAm99-001-001.grd.lmsk
queh-p-CAm99-001-001.sir.lmsk
queh-p-ChJ99-001-001.grd.lmsk
queh-p-ChJ99-001-001.sir.lmsk
queh-p-Eur99-001-001.grd.lmsk
queh-p-Eur99-001-001.sir.lmsk
queh-p-Grn99-001-001.grd.lmsk
queh-p-Grn99-001-001.sir.lmsk
queh-p-Ind99-001-001.grd.lmsk
queh-p-Ind99-001-001.sir.lmsk
queh-p-NAf99-001-001.grd.lmsk
queh-p-NAf99-001-001.sir.lmsk
queh-p-NAm99-001-001.grd.lmsk
queh-p-NAm99-001-001.sir.lmsk
queh-p-SAf99-001-001.grd.lmsk
queh-p-SAf99-001-001.sir.lmsk
queh-p-SAm99-001-001.grd.lmsk
queh-p-SAm99-001-001.sir.lmsk
queh-p-SAs99-001-001.grd.lmsk
queh-p-SAs99-001-001.sir.lmsk
queh-p-Sib99-001-001.grd.lmsk
queh-p-Sib99-001-001.sir.lmsk

Fig. 1. Observation Geometry

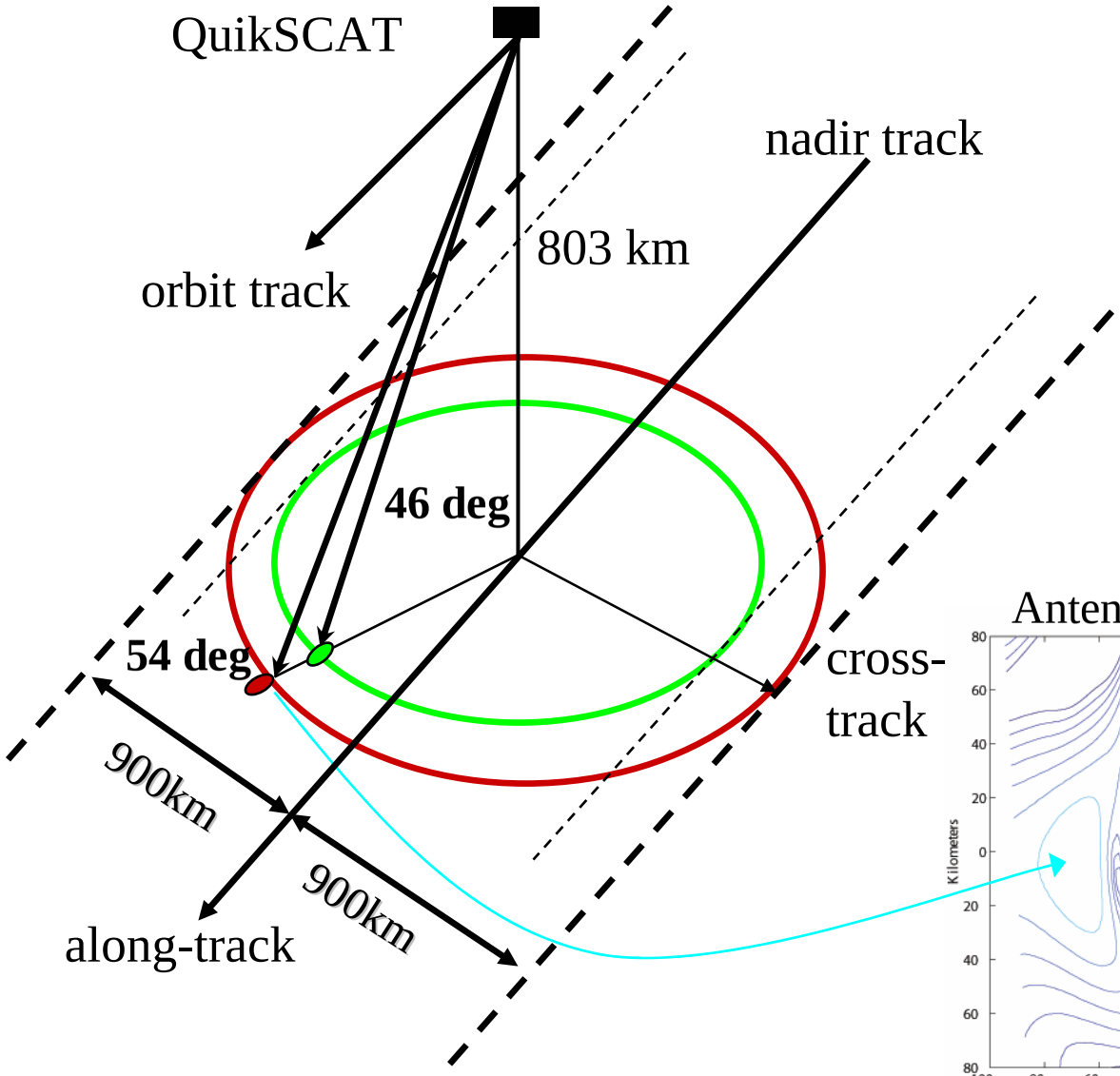

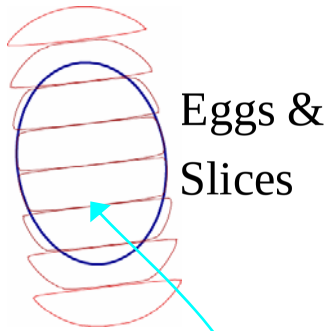

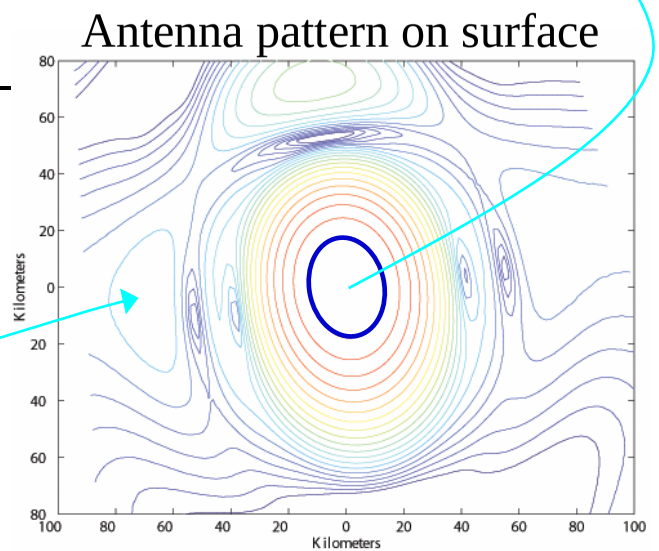

Fig. 2. SeaWinds geometry. (left) Swath diagram. (center) Contour plots of the antenna illumination patterns for egg and slice measurements. (right) Slice and egg comparison. Enhanced resolution grid illustration with single slice.

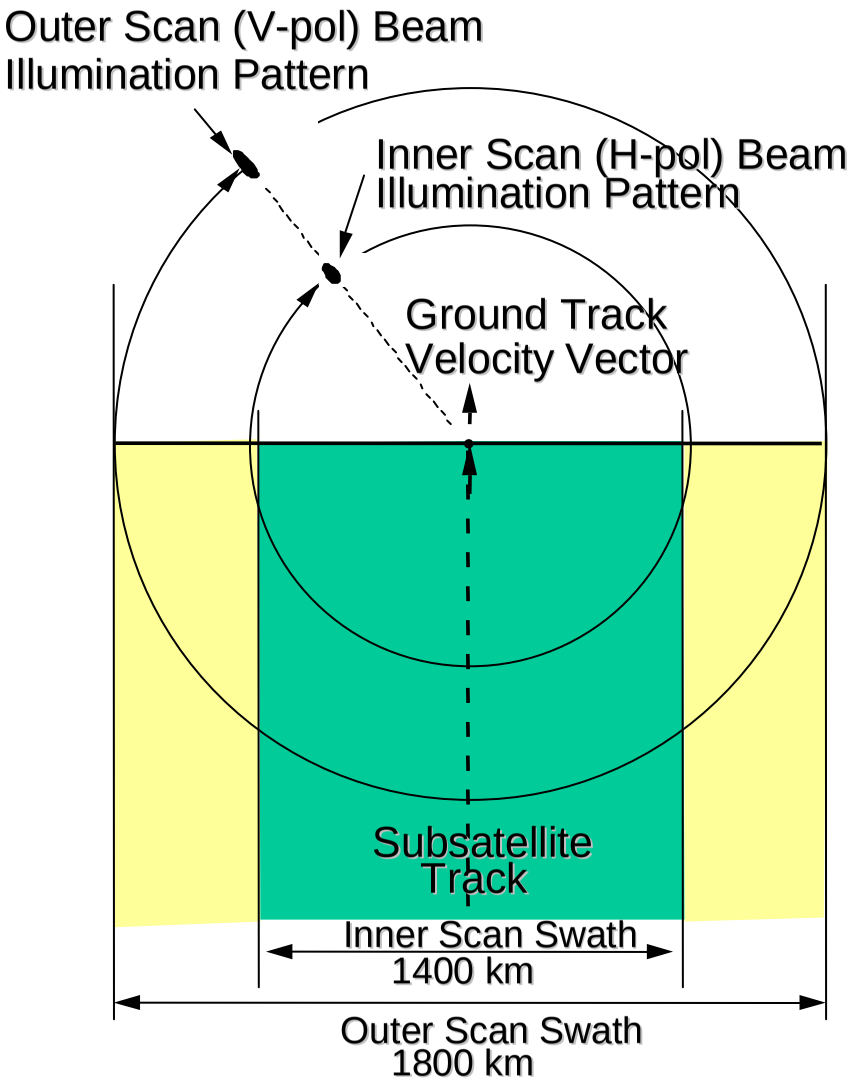

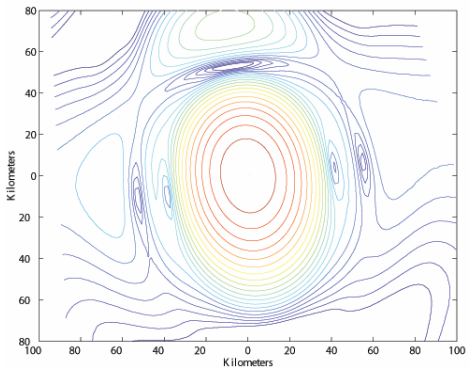

Egg
Response
24 x 31 km

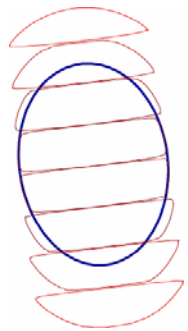

Slice & Egg
Response
Comparison

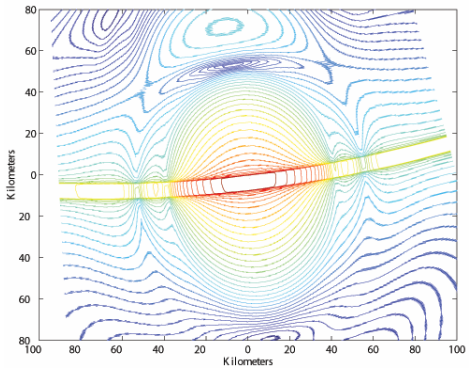

Example Slice
Response
~ 6 x 25 km

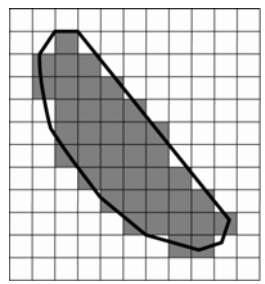

Enhanced
Resolution
Grid
Illustration

Fig. 3. Overlap of QuikSCAT slices for a few consecutive pulses during a single antenna rotation and several antenna rotations at two different orbit locations

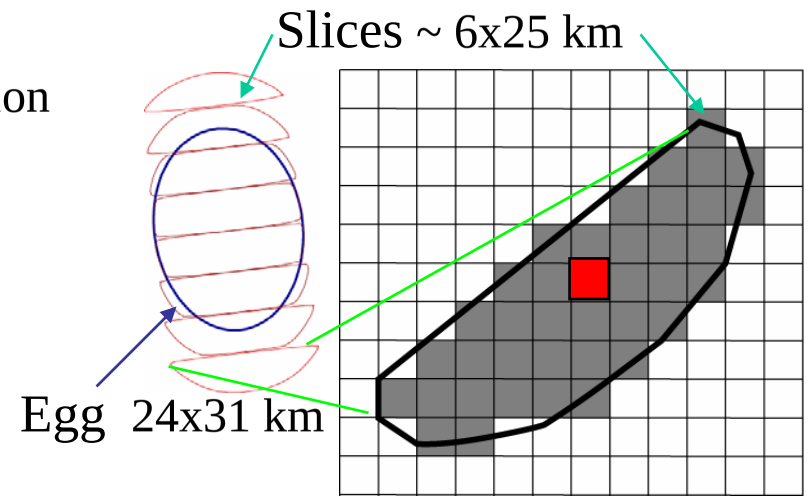

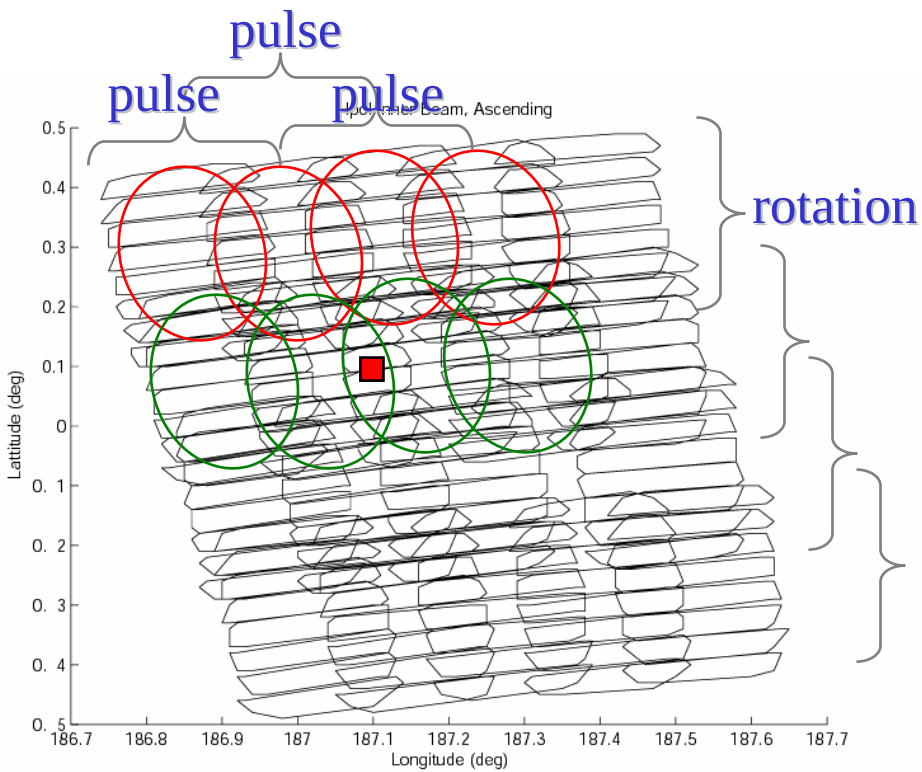

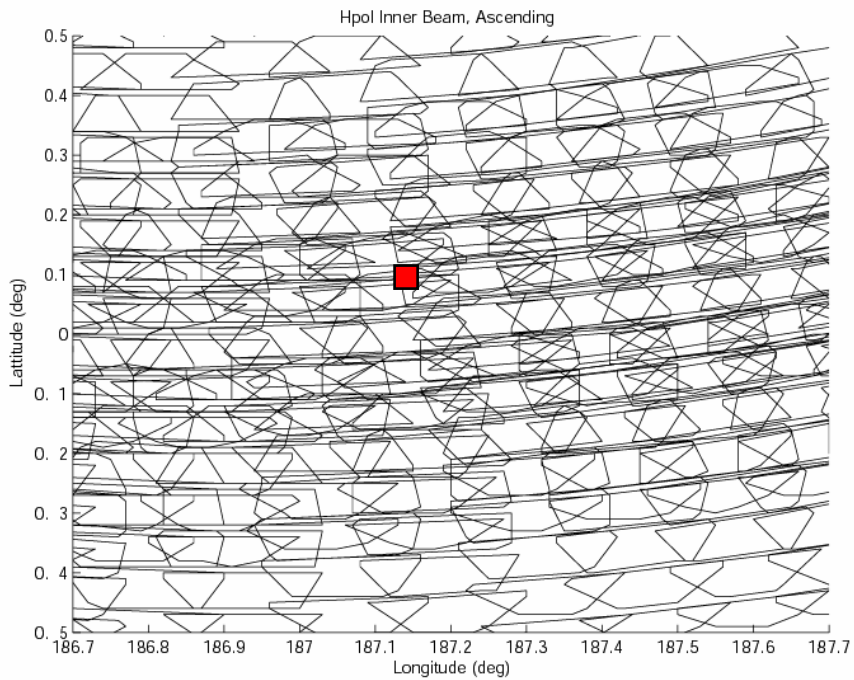

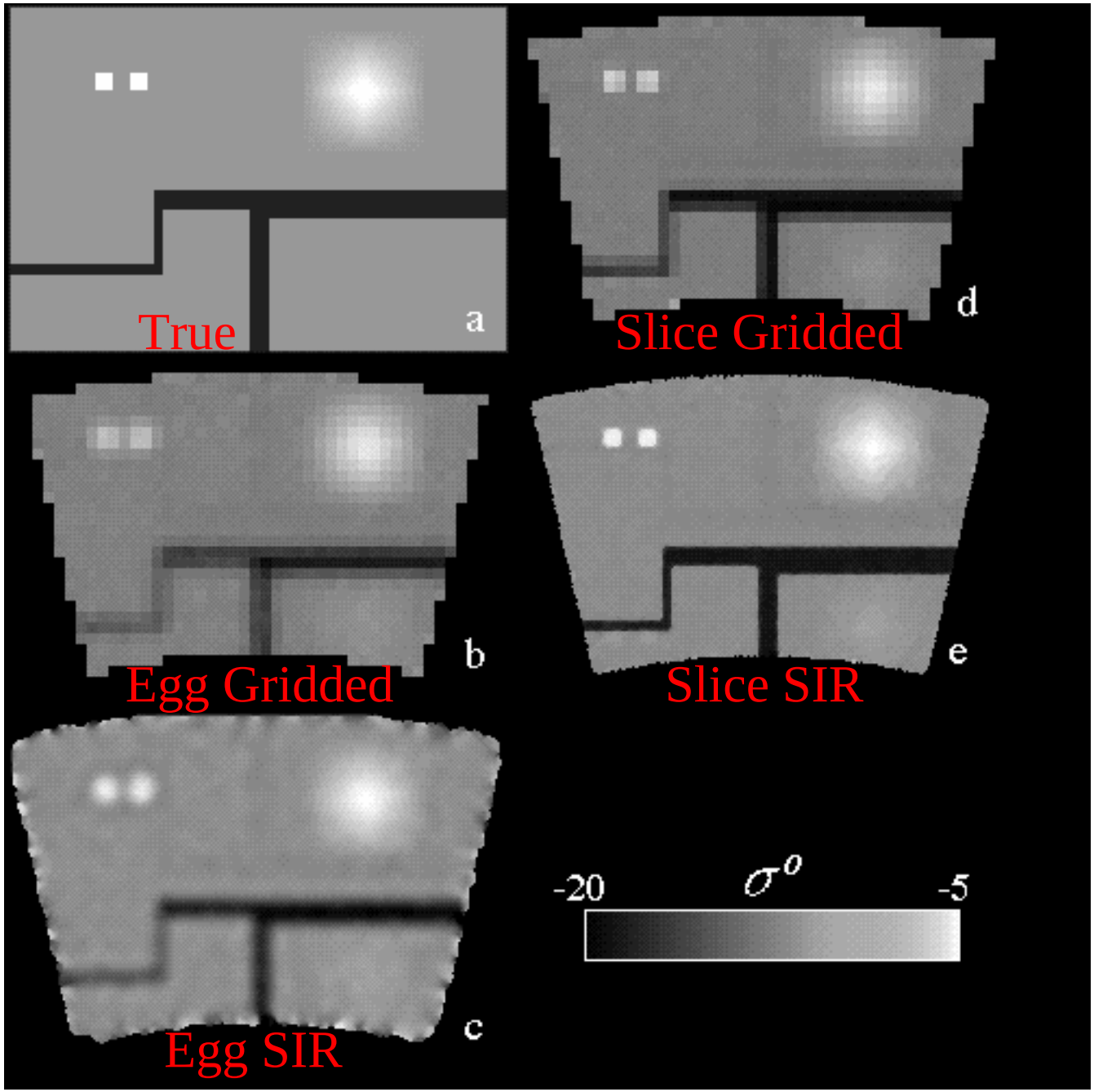

Fig. 4. SIR algorithm Simulation results. (a) Synthetic true image. (b) “drop in the bucket” grid image [non image] from eggs. (c) SIR image from egg measurements. (d) Grid image from slices [non image]. (e) SIR image from slices.

Fig. 5. Examples of polar region *A* images. These images have been ice masked.

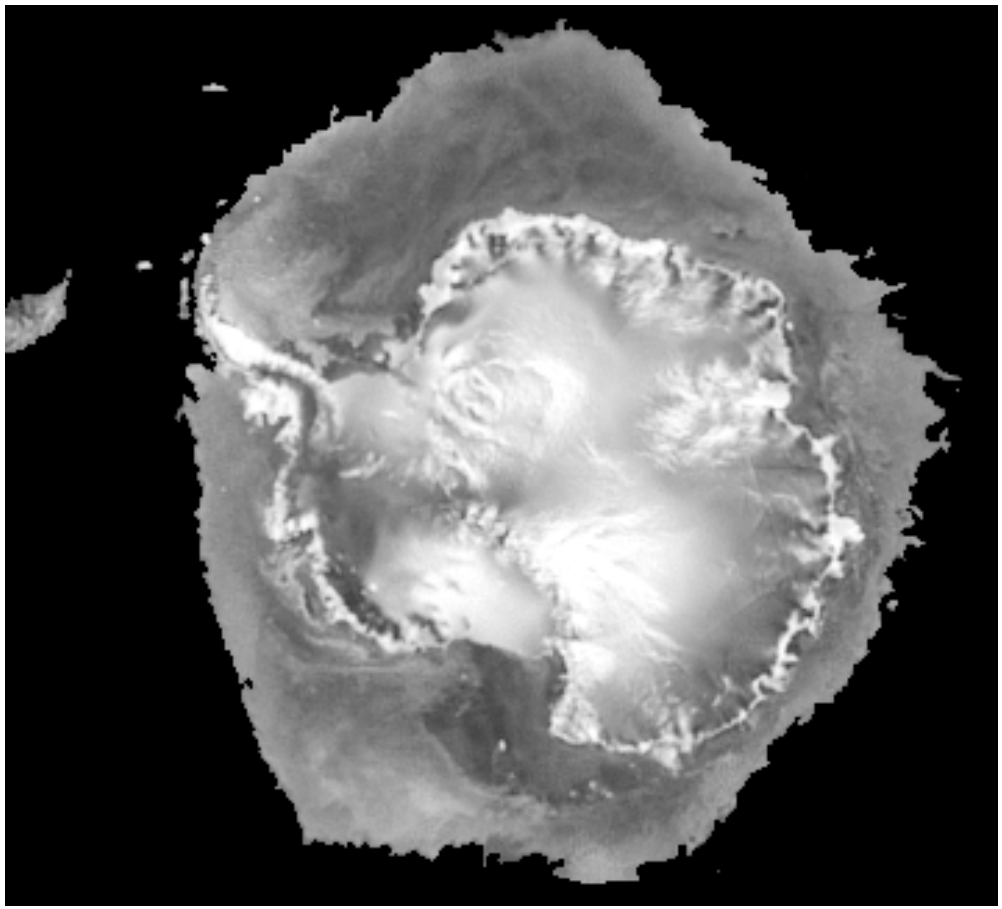

Ant (.imsk)

H-pol

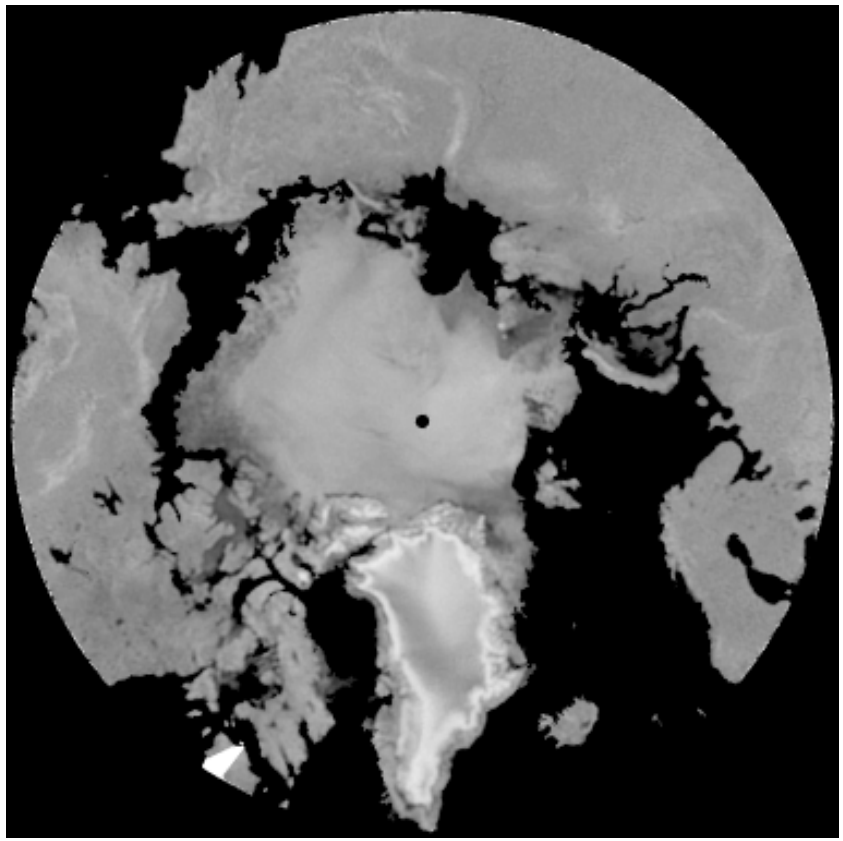

Arc (.imsk)

-30 dB *A* 0 dB

Fig. 7. Examples of QuikSCAT enhanced resolution land regions.
All images have been land or masked. Red boxes are shown in greater detail in later figures.

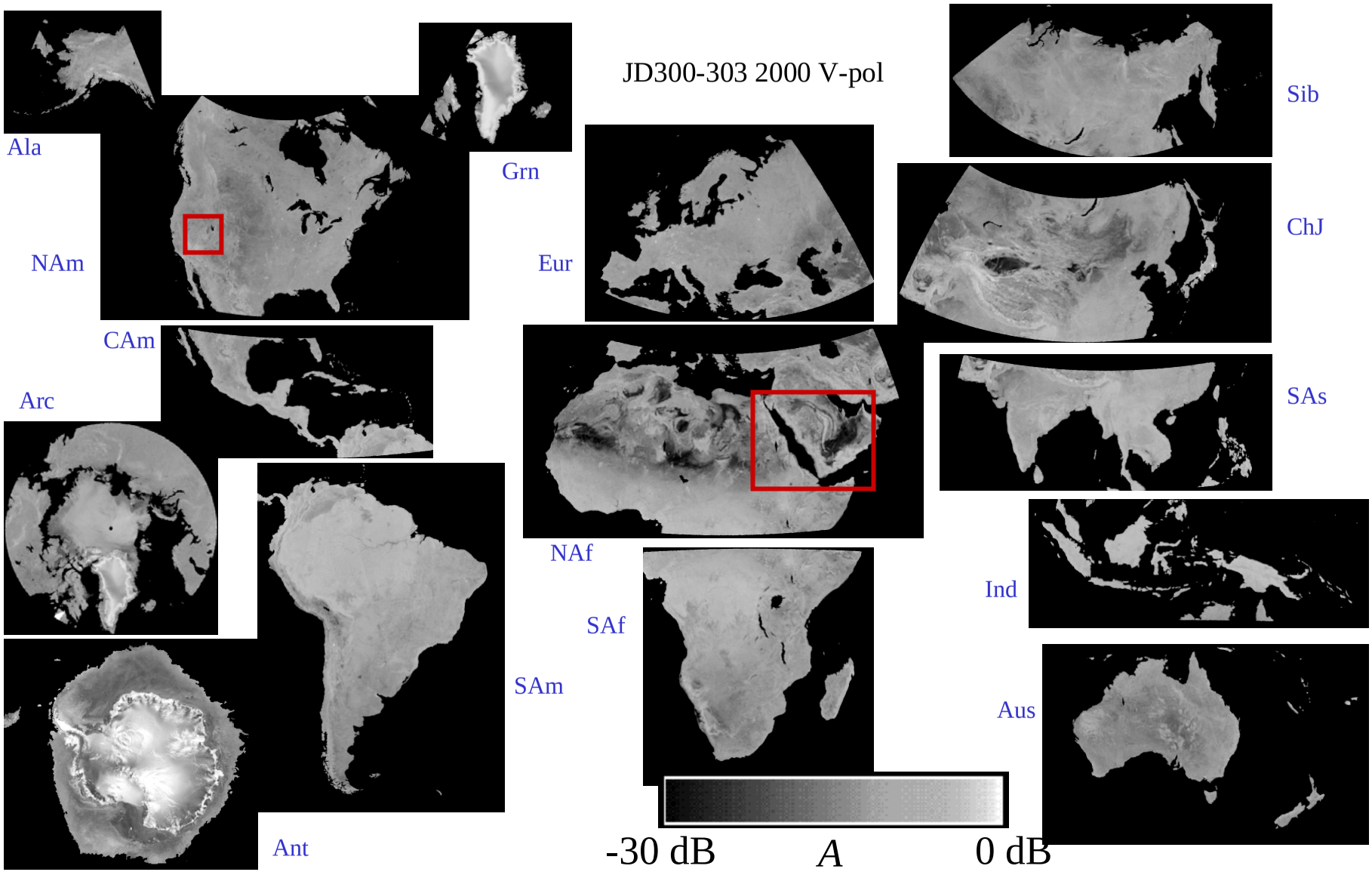

Fig. 8. Egg-based SIR enhanced-resolution image example.

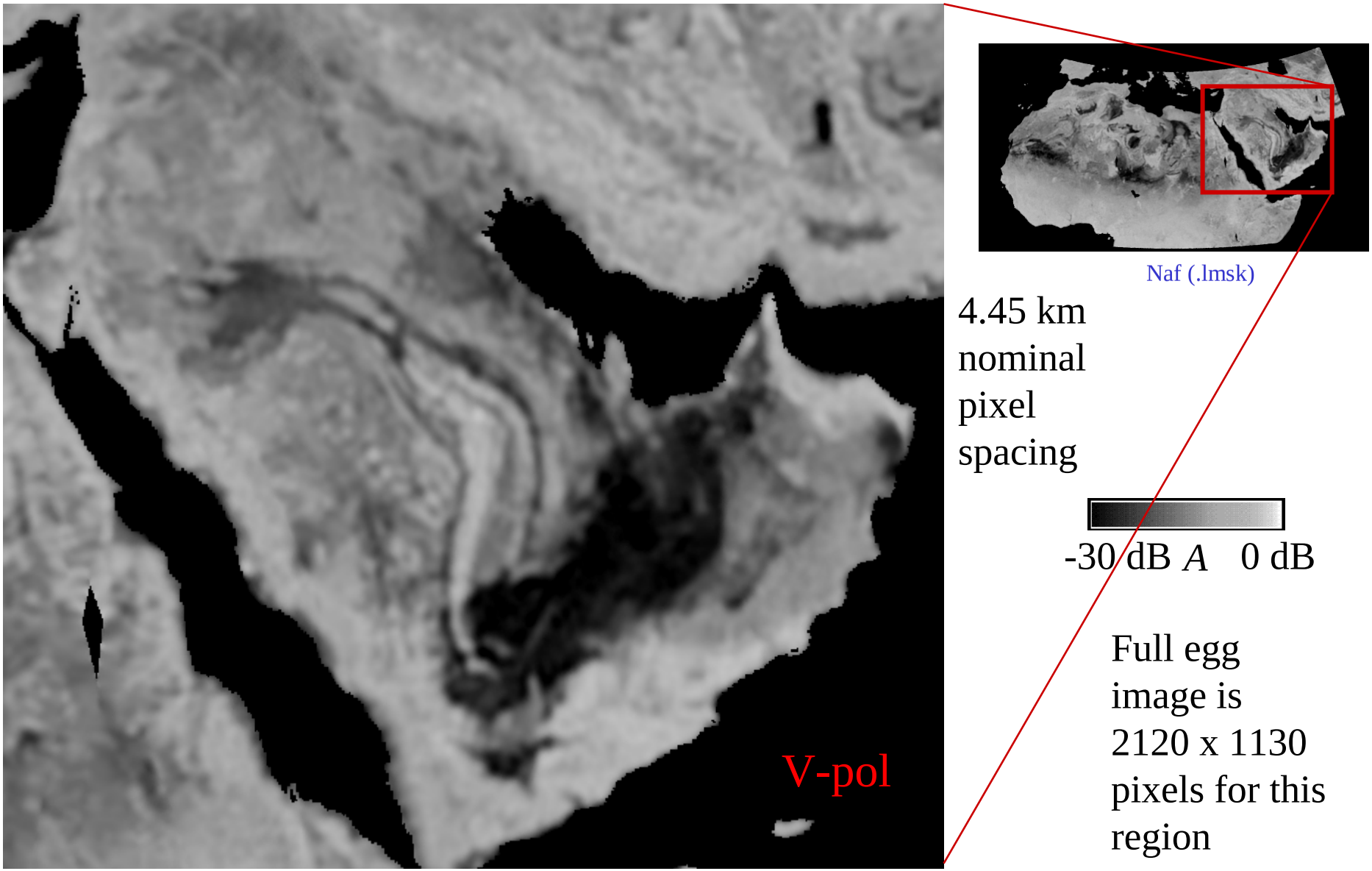

Fig. 9. Resolution comparison of various reconstruction types.

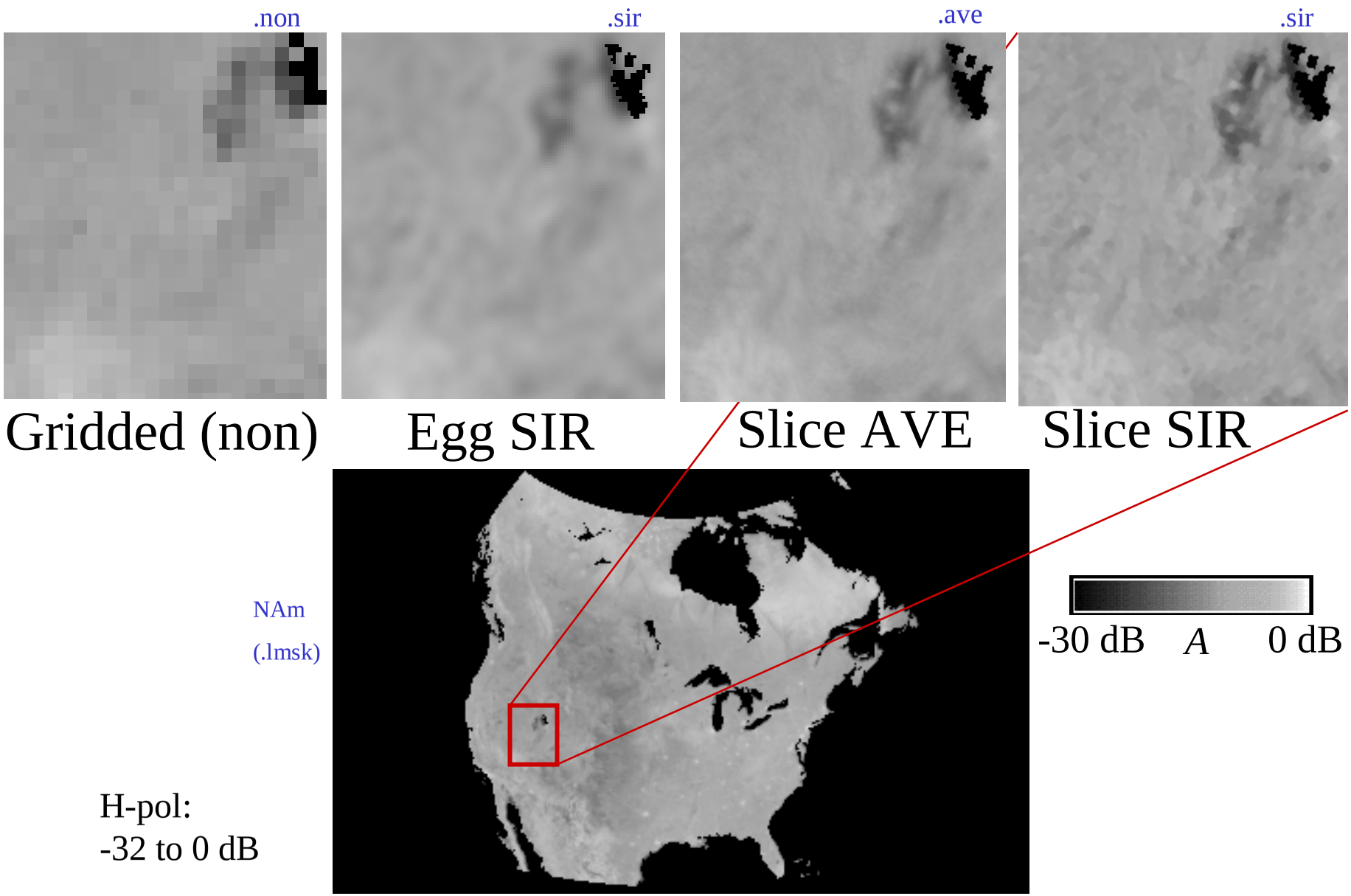

Fig. 10. Example ancillary products

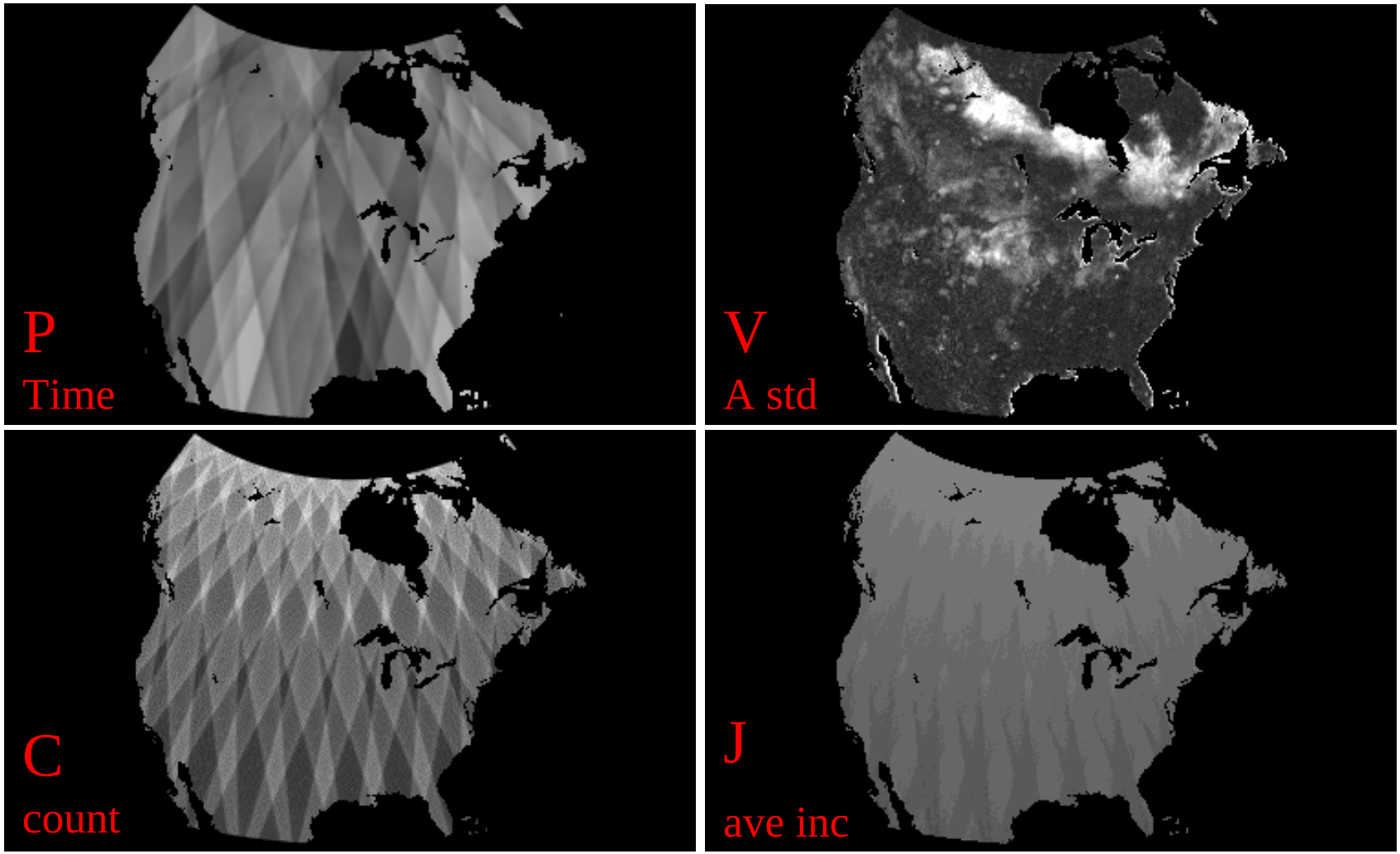

NAm(.lmsk)

H-pol

Fig. 11. Land mask and topography images

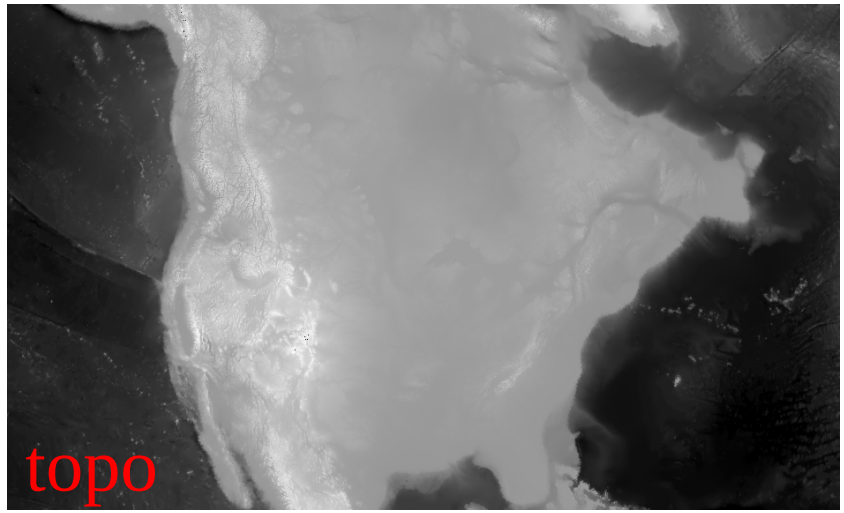

NAm

Fig. 12. SeaWinds Observes Land/Ice Surfaces of the Earth